Applied Catalysis B: Environmental 232 (2018) 436–445

Contents lists available at ScienceDirect

Applied Catalysis B: Environmental

journal homepage: www.elsevier.com/locate/apcatb

Evaluation of H_2O_2 electrogeneration and decolorization of Orange II azo dye using tungsten oxide nanoparticle-modified carbon

Edson C. Paz[a,e], Luci R. Aveiro[a], Victor S. Pinheiro[a], Felipe M. Souza[a], Verônica B. Lima[b,d], Fernando L. Silva[b,d], Peter Hammer[c], Marcos R.V. Lanza[b,d], Mauro C. Santos[a,*]

[a] LEMN - CCNH – Centro de Ciências Naturais e Humanas, UFABC – Universidade Federal do ABC, Rua Santa Adélia 166, Bairro Bangu, CEP 09.210-170 Santo André, SP, Brazil
[b] IQSC - Instituto de Química de São Carlos, USP - Universidade de São Paulo, Caixa Postal 780, CEP 13.566-590, São Carlos, SP, Brazil
[c] Instituto de Química, UNESP, Universidade Estadual Paulista, 14800-060 Araraquara, SP, Brazil
[d] Instituto Nacional de Tecnologias Alternativas Para Detecção, Avaliação Toxicológica e Remoção de Micropoluentes e Radioativos (INCT-DATREM), Instituto de Química, Unesp, 14800-900 Araraquara, SP, Brazil
[e] IFMA - Instituto Federal de Educação, Ciência e Tecnologia do Maranhão, Campus Açailândia, CEP 65.930-000 Açailândia, MA, Brazil

ARTICLE INFO

Keywords:
$WO_{2.72}$
Nanoparticles
H_2O_2
Electrogeneration
EAOPs
Dye decolorization

ABSTRACT

In this paper, we report on the development of a new catalyst for H_2O_2 electrogeneration for the preparation of a gas diffusion electrode (GDE) for water treatment by electrochemical advanced oxidation processes (EAOPs). Catalysts based on tungsten oxide nanoparticles on Vulcan XC72 and Printex 6L carbons were studied by X-ray diffraction (XRD), transmission electron microscopy (TEM), energy dispersive spectroscopy (EDS), X-ray photoelectron spectroscopy (XPS), contact angle measurements and oxygen reduction reaction (ORR) assays using a rotating ring-disk electrode (RRDE) system. The $WO_{2.72}$/Vulcan XC72 (1% w/w of W) catalyst was used for the construction of a GDE due to its notable performance in H_2O_2 electrogeneration, its good current efficiency for H_2O_2 electrogeneration and its lower energy consumption. Thus, the $WO_{2.72}$/Vulcan XC72 GDE cathode was combined with a Pt or boron-doped diamond (BDD) anode for the decolorization of 0.260 mM Orange II azo dye solutions by EAOPs. The decolorization efficiency was in the following sequence: photodegradation (PD) < Pt/anodic oxidation (AO) ≈ BDD/AO < BDD/electro-Fenton (EF) ≈ BDD/photoelectro-Fenton (PEF) < Pt/EF < Pt/PEF. The Orange II decolorization efficiency by Pt/PEF was equal to or higher than that reported in similar studies. Moreover, the results showed that an Orange II decolorization percentage of 77% in the PEF and EF processes with a Pt anode was due to the $WO_{2.72}$/Vulcan XC72 cathode, showing that this catalyst is a promising candidate for application in EAOPs.

1. Introduction

Large volumes of azo dye colored effluents are daily discharged into water bodies around the world [1]. However, conventional water treatments, such as biodegradation and physico-chemical treatments (coagulation/flocculation, adsorption and membrane separation) have been shown to be inefficient and/or of limited efficacy in dye removal [1,2]. On the other hand, electrochemical advanced oxidation processes (EAOPs) are considered to be good alternatives for aquatic decontamination. EAOPs allow the efficient degradation of almost all persistent organic pollutants in aqueous medium via the in situ generation of reactive oxygen species (ROS), such as hydroxyl radicals (·OH) [3–5]. This radical is able to react non-selectively with organic substances until its complete mineralization (transformation into CO_2, H_2O and inorganic ions) [3,6,7].

Recently, there have been increasing efforts in developing EAOPs based on in situ hydrogen peroxide production, such as electro-Fenton and photoelectro-Fenton, among others [3,8–10]. H_2O_2 is produced by the oxygen reduction reaction (ORR) two-electron pathway in carbonaceous cathodes, such as carbon-poly(tetrafluoroethylene) (PTFE) gas (O_2 or air) diffusion electrodes [4,6,11–14], carbon felt [15], reduced graphene oxide or graphene [16,17], carbon nanotubes [18], etc. However, the ORR can follow two different pathways: a 2-electron pathway, forming hydrogen peroxide or a hydroperoxide ion, or a 4-electron pathway, forming water or a hydroperoxyl ion [6,19].

Therefore, to produce H_2O_2 in acidic media, efficient electrocatalyst materials are fundamental, since the ORR presents slow kinetics [20] and a high overpotential. Carbonaceous materials, such as carbon

* Corresponding author.
E-mail address: mauro.santos@ufabc.edu.br (M.C. Santos).

https://doi.org/10.1016/j.apcatb.2018.03.082
Received 2 October 2017; Received in revised form 19 March 2018; Accepted 21 March 2018
Available online 23 March 2018
0926-3373/

black, are well-known cathodes for the reduction of oxygen to H_2O_2 [19,21] and an excellent support of electrocatalysts due to its high stability, large specific surface area, corrosion resistance, high potential for H_2 evolution, low catalytic activity for the decomposition of H_2O_2, non-toxicity and low cost [19,21,22].

In the last decade, our group and other researchers have been able to improve the electrocatalytic activity of carbon for the ORR by modification of different carbon varieties with metallic nanostructures [4,6,13,14,23,24], including WO_3 nanoparticles (NPs). Assumpção et al. [11] verified that Vulcan XC72R and Printex 6L WO_3 NP-modified carbons with a mass ratio of 1:100 (W:C) presented the best catalytic activity for H_2O_2 electrogeneration when compared to the supports without modification.

The modified carbon supports have been used to produce gas diffusion electrodes (GDEs) as cathodes in EAOPs, such as anodic oxidation, electro-Fenton and photoelectro-Fenton, among others [9]. The GDEs are advantageous for H_2O_2 electrogeneration due to the large contact areas among the cathode, oxygen and water [22]. Moreover, the modified carbon GDEs should show H_2O_2 electrogeneration at a lower energy consumption due to the reduced potential difference between electrodes during cathodic H_2O_2 generation.

Anodic oxidation (AO) is one of the EAPOs applied for polutant degradation [25]. Organic compounds are degraded by hydroxyl radicals formed by the oxidation of water, according to reaction (1) [3] or by direct oxidation on the anode surface [25]. The type of anode material strongly influences the performance of anodic oxidation [25]. Active anodes, such as Pt, usually exhibit low mineralization because most of the physisorbed M(·OH) is converted into the chemisorbed superoxide MO, which is a poor oxidant [25,26]. This behavior is minimized in the case of non-active anodes, such as boron-doped diamond (BDD), which has a higher efficiency to degrade organic pollutants [25,27].

$$M + H_2O \rightarrow M(^{\bullet}OH) + H^+ + e^- \quad (1)$$

Another very popular EAOP is electro-Fenton (EF). EF is based on the continuous supply of H_2O_2 by reaction (1) [3]. The organic compound is degraded by ·OH radicals formed by the Fenton reaction (2) between hydrogenated H_2O_2 and added Fe^{2+} ions at a pH of approximately 3 [28]. This reaction propagates through Fe^{2+} regeneration by the reduction of Fe^{3+} (Eq. (3)) [26]. In the photoelectro-Fenton (PEF) reaction, the solution is irradiated with artificial UVA light [26,29]. This radiation facilitates the degradation process of organic compounds due to the faster regeneration of Fe^{2+} and increased ·OH production induced by the photoreaction of $Fe(OH)^{2+}$ species (Eq. (4)) and the photolysis of complexes of Fe(III)-carboxylate (Eq. (5)) [8,12], in which carbon-centered radicals ($R^{\bullet}$) are also formed [30].

$$Fe^{2+} + H_2O_2 \rightarrow Fe^{3+} + {}^{\bullet}OH + OH^- \quad (2)$$

$$Fe^{3+} + e^- \rightarrow Fe^{2+} \quad (3)$$

$$Fe(OH)^{2+} + hv \rightarrow Fe^{2+} + {}^{\bullet}OH \quad (4)$$

$$Fe(OOCR)^{2+} + hv \rightarrow Fe^{2+} + CO_2 + R^{\bullet} \quad (5)$$

In the present work, $WO_{2.72}$ NPs were supported on Vulcan XC72 and Printex 6L carbons at a mass ratio of 1:100 (W:C) to evaluate the electrocatalytic activity for ORR and H_2O_2 electrogeneration. To the best of our knowledge, there is no report on the modification of Vulcan XC72 carbon with $WO_{2.72}$ NPs, as developed in this work. The modified Vulcan XC72 carbon with $WO_{2.72}$ NPs ($WO_{2.72}$/Vulcan XC72) was used for the preparation of the GDE. Subsequently, H_2O_2 produced was quantified using both the modified and unmodified GDE cathodes.This GDE was also used in the decolorization of Orange II dye solution by photodegradation, anodic oxidation, electro-Fenton and photoelectro-Fenton processes.

2. Materials and methods

2.1. Electrocatalysts preparation

The $WO_{2.72}$ nanoparticles supported on Vulcan XC72 (Cabot Corporation) or Printex 6L (Evonik-Degussa) carbon without any previous treatment were prepared by the polymeric precursor method (PPM) on the mass ratio 1:100 (W:C) [11,23]. All reagents used were purchased from Sigma–Aldrich.

2.2. X-ray diffraction (XRD)

All electrocatalysts were characterized by X-ray diffraction using a Rigaku-MiniFlex X-ray diffractometer with a continuous Cu Kα radiation source (2° min^{-1}) at intervals of 20–60°.

2.3. X-ray photoelectron spectroscopy (XPS)

The XPS analysis was carried out at a pressure of less than 10^{-7} Pa using a commercial spectrometer (UNI-SPECS UHV). The Al Kα line was used ($h\nu$ = 1486.6 eV), and the analyzer pass energy was set to 10 eV. The inelastic background of the W 4f, O 1s and C 1s high-resolution core-level spectra was subtracted using Shirley's method. The spectra were fitted without placing constraints using multiple Voigt profiles using the CasaXPS software. The width at half maximum (FWHM) varied between 1.3 and 2.0 eV, and the accuracy of the peak positions was ± 0.1 eV.

2.4. Transmission electron microscopy (TEM) and energy dispersive spectroscopy (EDS)

Images obtained by TEM were performed using a JEOL JEM-2100 electron transmission microscope operating at 200 kV. The samples for the TEM studies were prepared by placing nanodispersion droplets on a carbon-coated copper grid and evaporating the solvent at room temperature [31]. The EDS analyzes were performed using an EDS chemical microanalysis module coupled to a JEOL JSM-6010LA compact sweep electron microscope.

2.5. Contact angle measurements

The contact angle measurements of $WO_{2.72}$/Vulcan XC-72, $WO_{2.72}$/Printex 6L Vulcan XC-72 and Printex 6L electrocatalysts were performed using a goniometer (GBXTM digidrop). For this, solutions of all materials with concentration of 2.3 mg mL^{-1} (material/distilled water) were prepared and sonicated for 1 min in a cutting-edge ultrasound. First, 60-μL aliquots of each dispersion were deposited on a glassy carbon (GC) plate and dried under constant nitrogen gas flow (N_2, 99.99% White Martins) with the aim of forming a thin and homogeneous film on the GC substrate. Thereafter, 5 μL of distilled water was put on the formed film to determine the contact angles. Measurements were made in quintuplicate, and Windrop + + software was used.

2.6. Oxygen reduction reaction (ORR)

The ORR was studied using a RRDE system with a Pine Instruments rotating ring-disk consisting of a glass carbon disk (0.25 cm^2) and a ring of Au (0.055 cm^2) with an experimental collection efficiency of 0.28. The disk was coated with the electrocatalyst to form the electrode, as proposed by Paulus et al. [32]. A 1 cm^2 platinum plate and a Hg/HgO electrode were used as the counter and reference electrodes, respectively. A solution of 1.0 mol L^{-1} NaOH (100 mL) was used as the electrolyte and was prepared from an analytical grade reagent purchased from Sigma–Aldrich. All electrochemical measurements were conducted with an Autolab PGSTAT 302N potentiostat/galvanostat. For all electrochemical ORR analyses, the electrolyte was first saturated

with oxygen, and the oxygen flow was maintained on the electrolyte during the measurements. Measurements were performed in an undivided cell at a fixed scan rate of 5 mV s^{-1} at room temperature. These electrochemical measurements were conducted according to the procedure proposed by Assumpção et al. [11]. The rotation of the RRDE system ranged from 100 to 1600 rpm, and the experiments were controlled with Metrohm Autolab B.V. NOVA software.

2.7. Electrogeneration of H_2O_2 in a gas diffusion electrode

Based on the results obtained from the RRDE system, GDEs with a 3.0 cm^2 exposed area were constructed with $WO_{2.72}$/Vulcan XC72 and Vulcan XC72 with 20% (w/w) of a 60% aqueous dispersion of DuPont Teflon® PTFE TE 3859, as proposed by Forti et al. [11,14,33,34]. This GDE was supplied with O_2 at a pressure of 0.2 bar and used as a working electrode in an electrochemical cell to determine the true quantity of H_2O_2 produced by exhaustive electrolysis at different potentials. Ag/AgCl (Analyzer) and 7.5 cm^2 Pt electrodes were employed as the reference and counter electrodes, respectively. The distance between the anode and cathode was 1.0 cm. Electrolysis was performed in an undivided cell with an aqueous electrolyte (350 mL) containing 0.1 mol L^{-1} H_2SO_4 and 0.1 mol L^{-1} K_2SO_4 at 20 °C. The H_2O_2 was quantified by reacting 0.5 mL of the electrolyte containing H_2O_2 with 4 mL of a solution containing 2.4 × 10^{-3} mol L^{-1} $(NH_4)_6$ Mo_7O_{24} and 0.5 mol L^{-1} H_2SO_4 and absorption measured at 350 nm [11,34]. The H_2O_2 concentration was determined from a previously constructed analytical curve using a Varian Cary 50 instrument [11].

The ORR study by the RRDE system can be performed in an alkaline or acidic medium [11,33]. The quantification of H_2O_2 must be conducted in an acidic medium [35]. In the previous work of our group, the study with the RRDE system and the quantification of H_2O_2 were performed in the following media: alkaline electrolyte (1.0 mol L^{-1} NaOH) and acid electrolyte (0.1 mol L^{-1} H_2SO_4 and 0.1 mol L^{-1} K_2SO_4), respectively. Therefore, the mentioned tests of the present research were performed under the same conditions because this study was motivated by the results obtained in our previous studies. The maintenance of these variables is important to establish the relationships between the works already developed by our group.

2.8. Decolorization of azo dye Orange II solution

The experiments were carried out with 350 mL of a 0.260 mM (= 91.23 mg L^{-1}) Orange II solution (Sigma–Aldrich) in 0.1 M K_2SO_4 at 20 °C using an undivided cell with a 7.5 cm^2 BDD (thin-film from NeoCoat; substrate: polycrystaline Si, dopant amount: 2500 ppm) or a Pt anode and a 3 cm^2 $WO_{2.72}$/Vulcan XC72 GDE cathode. The distance between the anode and cathode was 1.0 cm. Ag/AgCl was the reference electrode. Pt/photoelectro-Fenton, Pt/electro-Fenton, BDD/photo-electro-Fenton, BDD/electro-Fenton, Pt/anodic oxidation, BDD/anodic oxidation and photodegradation were the processes carried out in this work. The best potential for H_2O_2 electrogeneration with a $WO_{2.72}$/Vulcan XC72 GDE cathode was −0.7 V vs Ag/AgCl. Thus, this potential was applied for the decolorization of Orange II dye solution. The cathode was supplied with O_2 at a pressure of 0.2 bar, except in anodic oxidation trials. The electro-Fenton and photoelectro-Fenton trials were performed at pH = 3 and the addition of 0.5 mM Fe^{2+}. In the photo-electro-Fenton trials, a UV lamp (λ_{max} = 254 nm/UVP 90-0012-01) immersed in the solution provided irradiation to the medium. In anodic oxidation trials, the cathode was supplied with N_2 at a pressure of 0.2 bar. The photodegradation was carried out using a mercury UV lamp of λ_{max} = 254 nm staying at a distance of 2 cm of the gas diffusion cathode. The specifications of the lamp are: one of the most popular Pen-Ray Lamps. Its simplicity of physical dimensions lends itself to a multitude of applications. Lamp's lighted length is 2.12″ (53.8 mm), overall length is 4.62″ (117.3 mm). Lamp emits Mercury spectrum with the primary energy at 254 nm. The nominal voltages are 800 V (starting) and 270 V (operating). Recommended power supply 99-0055-01 (or 99-0055-02).

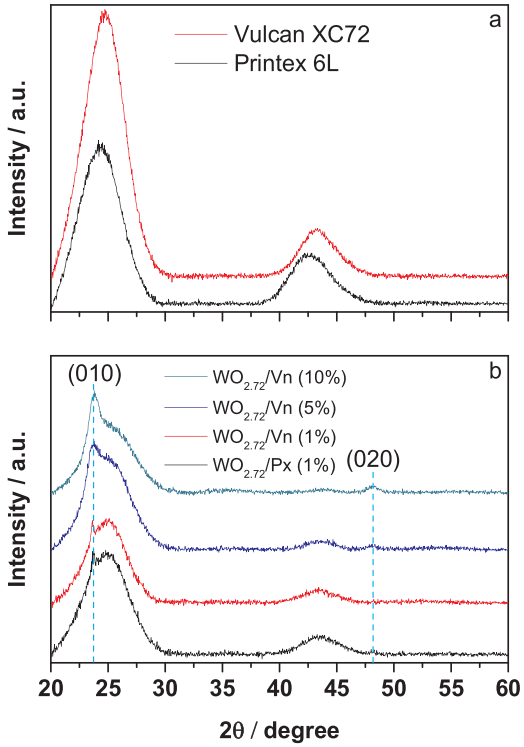

Fig. 1. a) XRD patterns of Vulcan XC72 and Printex 6L and b) 1% $WO_{2.72}$/Vulcan XC72 ($WO_{2.72}$/Vn), 1% $WO_{2.72}$/Printex 6L ($WO_{2.72}$/Px), 5% $WO_{2.72}$/Vulcan XC72 ($WO_{2.72}$/Vn) and 10% $WO_{2.72}$/Vulcan XC72 ($WO_{2.72}$/Vn) materials.

3. Results and discussion

3.1. X-ray diffraction (XRD) analysis

The crystalline structure of the tungsten-based electrocatalysts was studied by X-ray diffraction. Fig. 1a and b shows the diffraction peak patterns for the unmodified carbons and $WO_{2.72}$ NP-modified carbons at 1%, 5% and 10% W (w/w). The $WO_{2.72}$/Vn XRD patterns at 5% and 10% W (w/w) were determined to more clearly show the peaks obtained for the 1% W (w/w) material. In fact, as pointed out previously in the literature [36] the phase 020 presents a peak not well defined and with a small intensity even at for crystalline (pure) tungsten oxide.

The modification of the carbon with the incorporation of tungsten oxide was evidenced by the presence of the peaks assigned to the monoclinic phase $WO_{2.72}$ ($W_{18}O_{49}$) with (JCPDS Card no. 71-2450). The relatively small diffraction peaks located at 24.0 and 48.0 correspond to the (010) and (020) planes, respectively [36]. This phase appears when the thermal treatment is carried out in an oxygen deficient atmosphere [36]. The low crystallinity of the tungsten-based materials is probably related to lower temperatures of the thermal treatment [11,37].

3.2. X-ray photoelectron spectroscopy (XPS)

Fig. 2 displays the XPS survey spectra and the deconvoluted high-resolution C 1 s and W 4f core-level peaks of the tungsten oxide nanoparticles supported on Vulcan XC72 and Printex 6L carbon. The survey spectra show the presence of photoelectron peaks due to the ionization of the W 4f, W 4d and W 4p orbital. The C 1 s spectrum of both samples has been fitted with six components related to different chemical

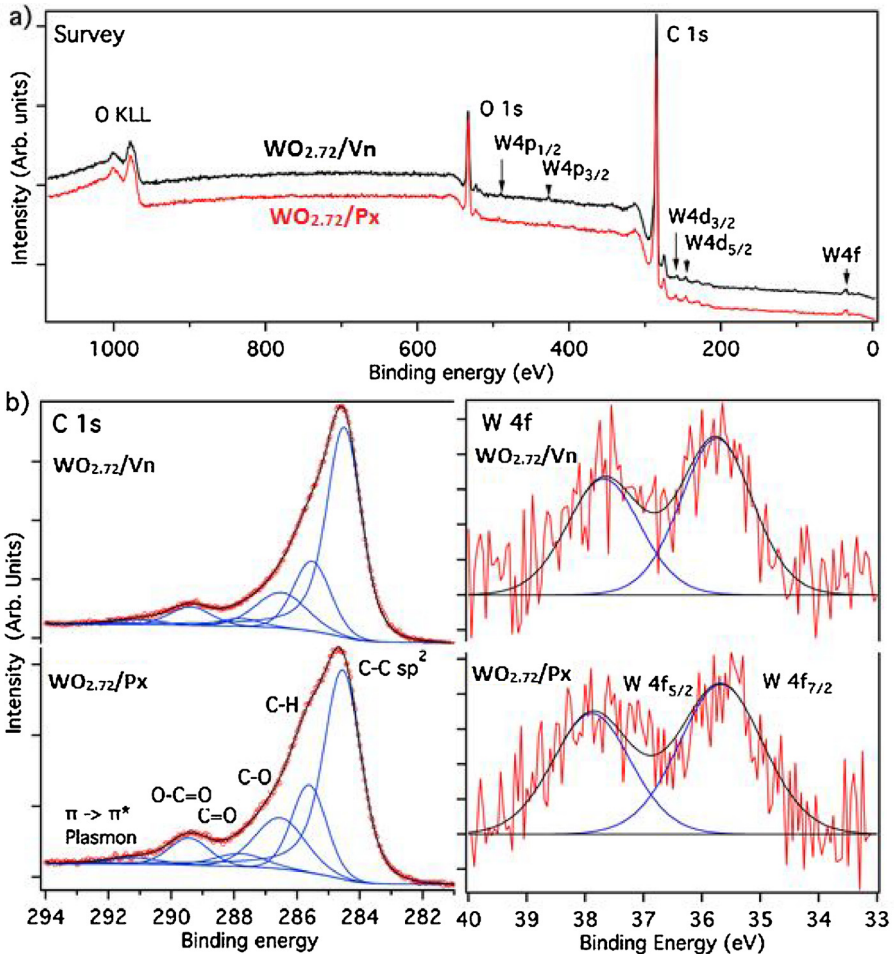

Fig. 2. a) XPS survey spectra of $WO_{2.72}$/Vulcan XC72 ($WO_{2.72}$/Vn) and $WO_{2.72}$/Printex 6L ($WO_{2.72}$/Px) electrocatalysts and b) the fitted high-resolution C 1s and W 4f spectra of the corresponding samples.

environments of carbon, showing the predominance of the aromatic C—C phase located at a binding energy of 284.5 eV. The C—H sub-peak at approximately 285.4 eV is related to the presence of C—H groups, indicating partial contribution from the amorphous phase in both carbon materials, as detected by XRD. The oxygenated carbon groups, which contribute to the high-energy tail of the spectrum, contain bridging C—O (286.5 eV) and carbonyl (287.8 eV) groups as well as a considerable concentration of carboxylic groups (289.4 eV) [38]. The latter groups preferentially form the surface layer, and thus, together with the C—O groups, they contribute to the elevated oxygen concentration in both samples, which was determined as 10.5 at.% for $WO_{2.72}$/Vulcan XC72 and 13.6 at.% for $WO_{2.72}$/Printex 6L. Compared with the $WO_{2.72}$/Printex 6L sample, the $WO_{2.72}$/Vulcan XC72 catalyst is characterized by a higher content of the aromatic phase and a slightly lower fraction of oxygenated groups.

Despite the noisy W 4f spectra of both samples (Fig. 2), a consequence of the relatively low tungsten content, the spectra were fitted with good precision using only one spin-orbit doublet attributed the W (VI) oxidation state, centered at a characteristic binding energy of 35.7 eV (W $4d_{7/2}$) [38]. It is interesting to note that the W 4f spin-orbit components of the $WO_{2.72}$/Printex 6L sample have a larger width (FWHM = 1.70 eV) than that observed for the $WO_{2.72}$/Vulcan XC72 catalyst (FWHM = 1.45 eV), indicating for the former has a slightly more disordered structure.

3.3. Transmission electron microscopy (TEM) and energy dispersive spectroscopy (EDS) analysis

The morphology of the $WO_{2.72}$ NPs of the synthesized electrocatalysts were studied by TEM. The micrographs were used to determine the shape and dispersion of the $WO_{2.72}$ NPs on the surface of the carbon [31]. This may help to understand the interaction between tungsten oxide and carbon and explain the influence of this metal on the modification of carbon and, consequently, on the electrocatalytic action. Fig. 3 shows images of the tungsten-based materials showing that the $WO_{2.72}$ NPs are spherical and are concentrated on certain parts of the carbon surface because a completely homogeneous dispersion across the carbonaceous area was not achieved. The $WO_{2.72}$ NPs supported on Vulcan XC72 carbon are more agglomerated than those on Printex 6L carbon.

The average mass percentage of the $WO_{2.72}$ NPs supported on the carbon surface was determined by EDS analysis. Knowing the density of the metallic nanoparticles present in the carbonaceous material is important because previous works developed by our and other research groups have observed the influence of the metal amount on the selectivity of the ORR pathway. It was found that carbon-based materials with lower metal content tend to favor the ORR by a 2-electron pathway [4,11,19,23]. Table 1 contains the average percentage of metals estimated by EDS analysis for the synthesized materials. The results are similar to the nominal values.

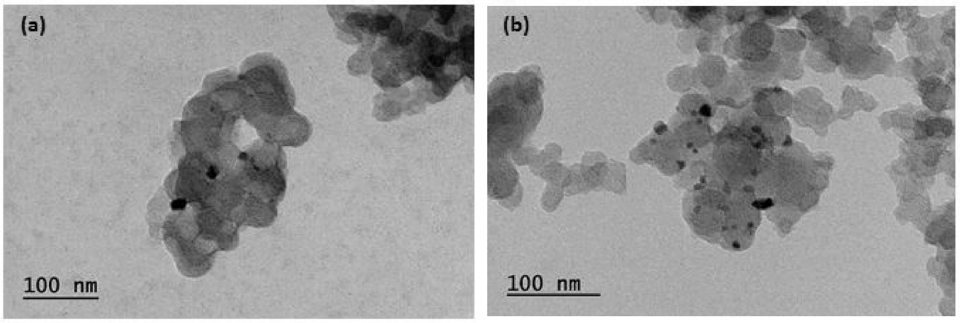

Fig. 3. (a) TEM image of $WO_{2.72}$ nanoparticles (1% w/w of W) anchored on Vulcan XC72 carbon. (b) TEM image of $WO_{2.72}$ nanoparticles (1% w/w of W) anchored on Printex 6L carbon.

3.4. Contact angle measurements

The surface tension of solids and liquids plays an important role in the processes in which adhesion, adsorption and wettability occur [39]. The wettability of the surface of the studied electrocatalysts was evaluated by measuring the contact angle of the water droplet, which is defined geometrically as the angle between the solid–liquid and liquid–vapor interfaces [40].

Table 1 shows the average contact angles for the unmodified and modified carbons. The unmodified carbons showed higher contact angle values compared to the modified carbons. Moreover, the change in contact angle was almost the same for $WO_{2.72}$/Vulcan XC72 ($\Delta\theta = 22.2°$) as for $WO_{2.72}$/Printex 6L ($\Delta\theta = 20.8°$) relative to the corresponding unmodified carbons. This is likely because the $WO_{2.72}$ NPs modified the surface of the carbons causing them to be more hydrophilic due to the increase of acidic oxygenated species [11,21].

3.5. Oxygen reduction reaction (ORR) study

The electrocatalytic activity, electron transfer number and current efficiency for hydrogen peroxide production for each electrocatalyst were studied using an RRDE system to determine the ORR pathway. Fig. 4 shows the polarization curves of the carbon-based materials, which have the same general shape and plateau of the well-defined limiting currents at less positive potential values indicating that the ORR is controlled by diffusion in that region [23].

All the synthesized materials presented ring currents greater than the respective reference materials (Printex 6L and Vulcan XC72), indicating an improvement of the catalytic activity for H_2O_2 electrogeneration by the incorporation of the $WO_{2.72}$ NPs on the carbon surface. $WO_{2.72}$/Printex 6L showed the highest ring current. The greatest relative increase in ring current was verified with $WO_{2.72}$/Vulcan XC72. The ring current limit of the modified Vulcan XC72 at −0.5 V vs Hg/HgO was 71 μA. This ring current is 42% greater than the current obtained for unmodified Vulcan XC72 (50 μA). On the other hand, $WO_{2.72}$/Printex 6L showed a 15% increase in the ring current in relation to unmodified Printex 6L. 76 and 66 μA were the ring currents obtained at −0.5 V vs Hg/HgO for $WO_{2.72}$/Printex 6L and unmodified Printex 6L, respectively. These results can be explained by the higher concentration of acidic oxygen groups [11] and the presence of Lewis and Brønsted acid sites on the carbon surface that arise due to the existence of W^{6+} [11,41]. They can increase the hydrophilicity of the carbon, as evidenced in contact angle measurements, favoring the adsorption of the oxygen molecule according to the Pauling model [11], which is selective for H_2O_2 generation [13,42]. Additionally, it was found that the $WO_{2.72}$ NPs shifted the ORR onset potential to lower potential values. This is another indication of the improvement in the catalytic activity for the ORR, which can signify energy savings in the process.

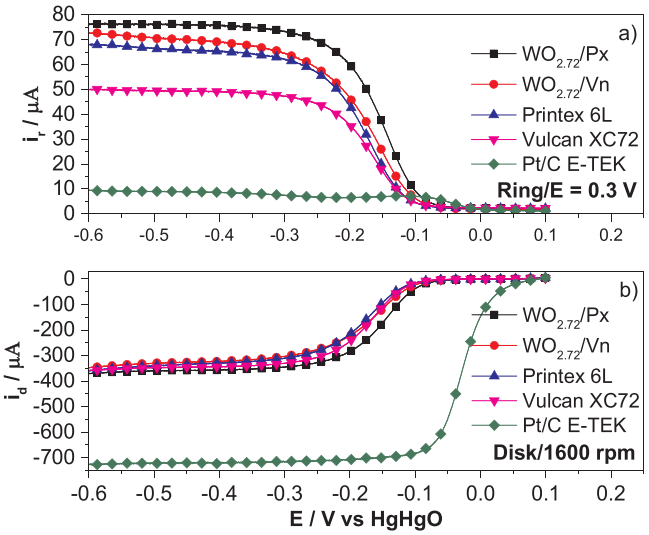

Fig. 4. Steady state polarization curves for the ORR determined using an RRDE system with a coated-disk electrode with $WO_{2.72}$/Vulcan XC72 ($WO_{2.72}$/Vn), $WO_{2.72}$/Printex 6L ($WO_{2.72}$/Px), Vulcan XC72, Printex 6L and Pt/C E-TEK in oxygen-saturated 1 mol L^{-1} NaOH at a scan rate of 5 mV s^{-1}. (a) Ring current E_r = 0.3 V. (b) Coated-disk current at 1600 rpm.

The Pt/C electrocatalyst presented the lowest ring current and twice the disk current, in relation to the other materials studied. This result was already expected because Pt is a reference material for the reduction of oxygen via a 4-electron pathway (water production) [23,43]. It

Table 1
The average contact angle values for water measured on the Vulcan XC72, Printex 6L, $WO_{2.72}$/Vulcan XC72 and $WO_{2.72}$/Printex 6L solid surfaces, and the average percentage with respect to the mass of tungsten in the $WO_{2.72}$/Vulcan XC72 and $WO_{2.72}$/Printex 6L electrocatalysts determined by EDS.

Samples	Contact angle (X ± A)/°	Composition by EDS (Y ± A)/%	Nominal percentage/%
$WO_{2.72}$/Vulcan XC72	22.2 ± 1.1	0.8 ± 0.1	1.0
$WO_{2.72}$/Printex 6L	20.8 ± 1.0	1.3 ± 0.2	1.0
Vulcan XC72	43.1 ± 2.1	–	–
Printex 6L	30.8 ± 0.6	–	–

X and Y are average values, and A is the average standard error. The % corresponds to the mass ratio (w/w) between tungsten and carbon.

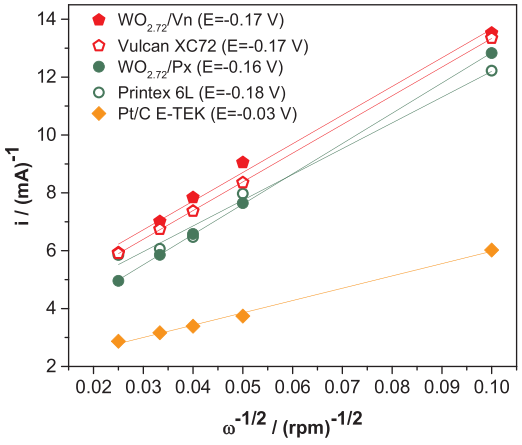

Fig. 5. Koutecky-Levich plots for the ORR with $WO_{2.72}$/Vulcan XC72 ($WO_{2.72}$/Vn), $WO_{2.72}$/Printex 6L ($WO_{2.72}$/Px), Vulcan XC72, Printex 6L and Pt/C E-TEK electrocatalysts.

was interesting to compare the polarization curve of Pt/C with the other electrocatalysts because it proves that the synthesized tungsten-based materials are selective for the ORR via a 2-electron pathway, and they are, therefore, promising for H_2O_2 electrogeneration.

The ORR data for all materials shown in Fig. 4 were analyzed using the Koutecky-Levich equation (Eq. (6)) [23]. The Koutecky-Levich plots of 1/i vs $1/\omega^{-1/2}$ were constructed from the curves of the disk at different rotation speeds [44]: 100, 400, 625, 900 and 1600 rpm.

$$\frac{1}{i} = \frac{1}{i_k} + \frac{1}{i_d} = \frac{1}{nFAkC^0} + \frac{1}{\{0.62nFAD_{O_2}^{\frac{2}{3}}\nu^{-\frac{1}{6}}C^0\omega^{\frac{1}{2}}\}} \quad (6)$$

where i is the measured current; i_k and i_d are the kinetic and diffusion limited currents, respectively; k is the rate constant for the ORR; F is Faraday's constant (96,484 C mol^{-1}); A is the effective projected area covered with the catalyst; ω is the rotation rate; C^0 is the saturated concentration of oxygen in the bulk solution; D_{O_2} is the diffusion coefficient of oxygen; and ν is the kinematic viscosity of the solution.

Fig. 5 shows the Koutecky-Levich plots, demonstrating that the lines corresponding to the $WO_{2.72}$/C NPs materials have similar slopes to the Vulcan XC72 carbon and Printex 6L carbon and larger line slopes than of the Pt/C E-TEK, as shown in Table 2. The K–L slope is inversely proportional to the electron transfer number in the ORR [45]. The linearity and parallelism between the lines of the $WO_{2.72}$/C materials and carbon indicate that the ORR mechanism is similar, exhibiting first-order kinetics [13,45]. As a result, carbon and Pt/C are reference materials for the two- and four-electron pathways in the ORR, respectively [11]. Results indicate that the ORR process using $WO_{2.72}$/C materials follows the two-electron pathway, which corresponds to the data presented by the polarization curves of the RRDE system shown in Fig. 4. Moreover, extrapolation of the K–L plot shows no intercept at zero, suggesting that the ORR occurs under mixed control [13].

The H_2O_2 (H_2O_2%) and H_2O (H_2O%) generation percentages and the electron transfer number (n_t) from the polarization curves obtained at 1600 rpm for all the electrocatalysts are described in the following equations [32,46]:

$$H_2O_2\% = \frac{200 \bullet i_r/N}{i_d + i_r/N} \quad (7)$$

$$H_2O\% = 100 - H_2O_2\% \quad (8)$$

$$n_t = \frac{4 \bullet i_d}{i_d + i_r/N} \quad (9)$$

where i_r is the ring current, I_d is the disk current and N is the current collection efficiency of the Au ring (N = 0.28).

The values of H_2O_2%, H_2O% and n_t for the electrocatalysts studied are shown in Table 2. These results show that the $WO_{2.72}$/Vulcan XC72 and $WO_{2.72}$/Printex 6L materials present a higher percentage of H_2O_2 production, and the electron transfer number during the ORR was close to 2. The results shown in Table 2 corroborate and complement the results obtained from the polarization curves and the K–L plots, which provided additional information for the selection of the most promising material for hydrogen peroxide formation.

Electrochemical analyses showed that $WO_{2.72}$/Vulcan XC72 and $WO_{2.72}$/Printex 6L had similar activities. The $WO_{2.72}$/Vulcan XC72 was selected for the preparation of the GDE because it showed the greatest relative increase in the ring current compared to the current obtained with unmodified carbon. Additionally, there are few H_2O_2 electrogeneration studies with Vulcan XC72 in the literature. Moreover, the Vulcan XC72 carbon is less expensive than Printex 6L carbon.

Table 2
Percentage of H_2O_2 and H_2O, and the electron transfer number and K–L slopes for $WO_{2.72}$/Vulcan XC72, $WO_{2.72}$/Printex 6L, Vulcan XC72, Printex 6L and Pt/C E-TEK electrocatalysts.

Samples	% H_2O_2	% H_2O	Electron number	K-L slopes
$WO_{2.72}$/Printex 6L	86	14	2.3	105 (E = −0.16 V)
$WO_{2.72}$/Vulcan XC72	87	13	2.3	99 (E = −0.17 V)
Printex 6L	82	18	2.4	90 (E = −0.18 V)
Vulcan XC72	67	33	2.7	99 (E = -0.17 V)
Pt/C E-TEK	8	92	3.8	43 (E = −0.03 V)

3.6. Electrogeneration of H_2O_2 in a gas diffusion electrode

The quantification of H_2O_2 at different cathodic potentials is necessary because it allows for the determination of the best potential for H_2O_2 production at a lower energy cost. Fig. 6(a) shows the concentration of H_2O_2 electrogenerated in different potentials applied as a function of time using Vulcan XC72 and $WO_{2.72}$/Vulcan XC72 GDEs. The electrolysis results confirm the ORR study results. The production of hydrogen peroxide by the $WO_{2.72}$/Vulcan XC72 GDE is higher than that produced by the Vulcan XC72 GDE at all potentials studied, as shown in Fig. 6(a). Moreover, the concentration of H_2O_2 produced increases with potentials up to −0.7 V vs Ag/AgCl. From this potential, there is a decrease in the concentration of electrogenerated H_2O_2. The H_2O_2 production decreases at high cathodic potentials due to the occurrence of the reduction of H_2O_2 to H_2O and the H_2 evolution reaction which is a side reaction and limits the ORR to generate H_2O_2 [47]. Moreover, the ORR by the 4-electron pathway is favored [6]. Fig. 6(b) shows the concentration of H_2O_2 electrogenerated at a potential of −0.7 V vs Ag/AgCl as a function of time using $WO_{2.72}$/Vulcan XC72 GDE after 3 h and 37 h. These results indicate the good stability of $WO_{2.72}$/Vulcan XC72 GDE, because after 37 h of electrode use in photoelectro-Fenton and electro-Fenton processes, it showed a loss of only 6% of hydrogen peroxide electrogeneration.

Fig. 7 shows the concentration of H_2O_2 produced and the current efficiency (CE) for the electrogeneration of H_2O_2 after 120 min of electrolysis. The H_2O_2 generation by the $WO_{2.72}$/Vulcan XC72 GDE, (e.g., 479.1 mg L^{-1}) is three times higher than that produced by the unmodified Vulcan XC72 GDE (160.5 mg L^{-1}) at −0.7 V vs Ag/AgCl, potential with higher H_2O_2 production. Thus, the following electrodegration using $WO_{2.72}$/Vulcan XC72 GDE was carried out applying this potential.

The CE was determined using Equation 10 [48]. The current efficiency at the potential −0.7 V vs Ag/AgCl of the $WO_{2.72}$/Vulcan XC72 GDE (41.9%) was 2.6 times higher than the unmodified Vulcan XC72 GDE (16.4%). The CE for H_2O_2 electrogeneration obtained with $WO_{2.72}$/Vulcan XC72 GDE (41.9%) was higher than obtained by Xia et al. [48] using 0.5 L of solution, which is a volume closer to that used in our work (0.35 L). Xia et al. [48] obtained an EC equal to 34.6% and

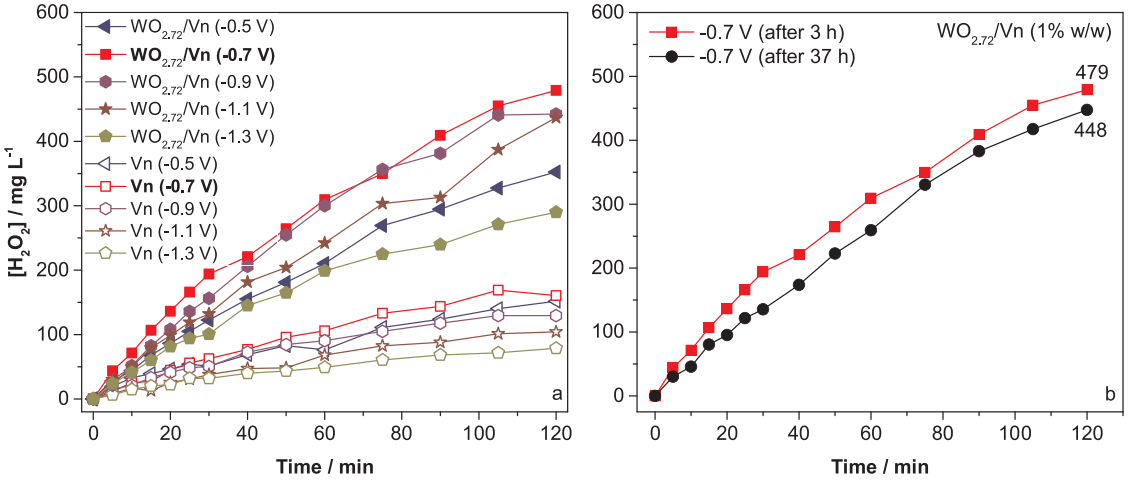

Fig. 6. a) H_2O_2 concentration as a function of electrolysis time at different applied potentials using $WO_{2.72}$ NPs supported on Vulcan XC72 (Vn). b) H_2O_2 concentration at −0.7 V vs Ag/AgCl after the use of $WO_{2.72}$/Vulcan XC72 GDE at 3 h and 37 h. Supporting electrolyte: 0.1 mol L^{-1} K_2SO_4 and 0.1 mol L^{-1} H_2SO_4. O_2 pressure = 0.2 bar.

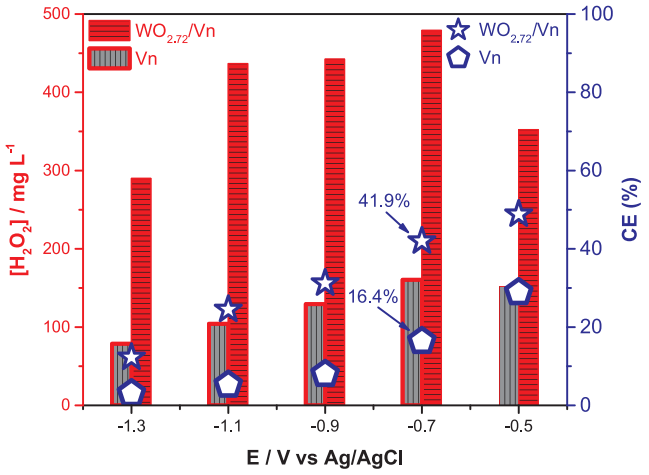

Fig. 7. Final concentrations of H_2O_2 and the current efficiency for electrogeneration of H_2O_2 obtained in 350 mL of 0.1 mol L^{-1} K_2SO_4 and 0.1 mol L^{-1} H_2SO_4, following 120 min of electrolysis using a GDE constructed with Vulcan XC72 and a GDE constructed with Vulcan XC72 modified with $WO_{2.72}$ nanoparticles.

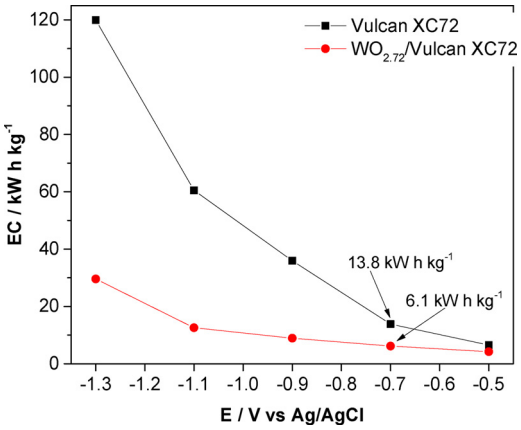

Fig. 8. Energy consumed in the electrogeneration of hydrogen peroxide by electrolysis with gas diffusion electrodes $WO_{2.72}$ NP-modified Vulcan XC72 carbon or unmodified Vulcan XC72 carbon.

96.0%, respectively, when working with 0.5 L and 2.0 L. Thus, we believe that the CE of $WO_{2.72}$/Vulcan XC72 GDE is not higher because a smaller solution volume favors the decomposition of H_2O_2 [48].

$$CE\ (\%) = \frac{z \bullet F \bullet [H_2O_2] \bullet V}{M_{H_2O_2} \bullet I \bullet t} \times 100 \quad (10)$$

where $[H_2O_2]$ is the concentration of H_2O_2 (g L^{-1}), F is the Faraday constant (96,485 C mol^{-1}), z is the number of electrons transferred for the reduction of oxygen to H_2O_2, V is the solution volume (L), $M_{H_2O_2}$ is the molar mass of H_2O_2 (34.01 g mol^{-1}), I is the applied current (A), and t is the electrolysis time (s).

In addition to the concentration of formed H_2O_2, it is important to know the amount of energy consumed during its formation from the ORR by the electrochemical process [14]. The energy consumption (EC, expressed in the units of kWh kg^{-1}) can be calculated [14]:

$$EC = \frac{i \bullet E_{cel} \bullet t}{1000m} \quad (11)$$

where i represents the current (A), E_{cel} is the cell potential (V), t is the time (h), and m is the mass of hydrogen peroxide formed (kg).

Fig. 8 shows the energy consumption (EC) for H_2O_2 generation at the applied potentials after 120 min of electrolysis using the Vulcan XC72 and $WO_{2.72}$/Vulcan XC72 (1% w/w of W) GDEs. An increase in energy consumption is shown as a function of the increase in applied potential, which was already expected. It can also be seen that the increase in energy consumption is higher with the unmodified carbon GDE. In the best potential for H_2O_2 generation (−0.7 V vs Ag/AgCl), the EC values of 13.8 kWh kg^{-1} and 6.1 kWh kg^{-1} were obtained for the unmodified and modified carbon GDEs, respectively. The modification of carbon with $WO_{2.72}$ NPs resulted in a 55.8% reduction in energy consumption for the generation of 1 kg of H_2O_2. This result also agrees with the results of the ORR study in which a shift of the ORR onset potential to lower potential values was observed when the ORR was performed with the $WO_{2.72}$/Vulcan XC72 electrode.

The results obtained from electrolysis showed that the $WO_{2.72}$/Vulcan XC72 electrocatalyst is promising for ORR by the 2-electron pathway with H_2O_2 electrogeneration rate higher than other studies reported in the literature [6,33,47], good current efficiency for electrogeneration of H_2O_2 and a lower energy cost compared to unmodified Vulcan XC72.

3.7. Decolorization of azo dye Orange II solution

Orange II azo dye, also called Acid Orange 7 or Acid Orange A, is widely used in the textile, food, cosmetics, leather and paper industries,

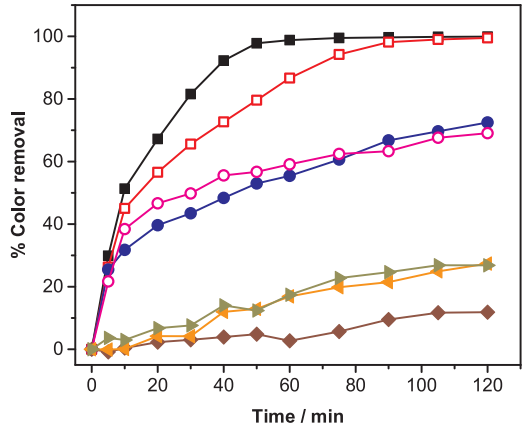

Fig. 9. Decolorization efficiency of the 0.260 mM Orange II solution (350 mL) by Pt/photoelectro-Fenton (■), Pt/electro-Fenton (□), BDD/photoelectro-Fenton (●), BDD/electro-Fenton (○), Pt/anodic oxidation (►), BDD/anodic oxidation (◄) and photodegradation (♦) processes using a $WO_{2.72}$/Vulcan XC72 GDE cathode.

among others [1,49]. The concentration of Orange II azo dye found in industrial wastewaters corresponds to 10 to 50 mg L^{-1} [50–52].

Decolorization was performed with a $WO_{2.72}$/Vulcan XC72 GDE cathode and Pt or BDD anode. A series of electrolysis tests was conducted to evaluate the performance of the Pt/modified carbon and BDD/carbon modified electrode pairs for application in the decolorization of Orange II dye solutions. The efficiency of the anodes was analyzed and compared under the same conditions to optimize the decolorization of Orange II solution. All experiments were performed with 350 mL of a 0.260 mM (= 91.23 mg L^{-1}) Orange II solution at 20 °C [3].

The color removal percentage or decolorization efficiency for the tests performed was calculated from Eq. (12) [1]:

$$\%\,\text{Color removal} = \frac{A_0 - A_t}{A_0} \times 100 \tag{12}$$

where A_0 and A_t are the absorbance at initial time and time t, respectively, at λ_{max} = 485 nm for Orange II [1,53].

Fig. 9 shows the results of the decolorization of the 0.260 mM Orange II solution at λ_{max} = 485 nm for different electrolysis times by photodegradation (PD), anodic oxidation (AO), electro-Fenton (EF) and photoelectro-Fenton (PEF) processes. Photodegradation and anodic oxidation removed only 12% and 27% of the coloration after 120 min of electrolysis, respectively. This poor decolorization ability is due to the mechanism of formation of oxidizing species. Anodic oxidation using the Pt or BDD anode showed similar results of decolorization. In anodic oxidation, the organic compound is degraded due to the hydroxyl radicals formed on the anode surface from the oxidation of water, according to reaction (1) [3].

The electro-Fenton and photoelectro-Fenton processes with a BDD anode presented similar results. After 120 min of electrolysis, 69% and 72% of the Orange II color were removed by the electro-Fenton and photoelectro-Fenton, respectively. These results are due to reactions (1)–(5) [3,53–55].

The electro-Fenton and photoelectro-Fenton processes with a Pt anode presented higher efficiency in the decolorization of the Orange II azo dye solution, in which 100% color removal occurred after 120 and 75 min of electrolysis, respectively, as shown in Fig. 9. The faster color removal by the Pt/photoelectro-Fenton can be explained by the occurrence of additional reactions (4) and (5), which provide the complexed Fe^{2+} ion [54,55]. Most of the studies conducted with the objective of comparing the performance of Pt and BDD anodes in the degradation of organic pollutants in wastewater showed the superiority of BDD independently of the EAOP [22]. However, surprisingly, the Pt anode in the photoelectro-Fenton and electro-Fenton processes was better than the BDD under the same conditions. This superiority of Pt can be attributed to faster oxidation of Fe^{2+} to Fe^{3+} on the BDD anode surface (Eq. (13)) together with the destruction of Fe^{2+} by the persulfate ion to obtain Fe^{3+} and sulfate on the BDD anode (Eq. (14)), decreasing the amount of Fe^{2+} to produce ·OH by Fenton's reaction (2) [22,56]. A study by Zazou et al. [3] on the degradation of chlorobenzene by the electro-Fenton process also showed the superiority of Pt anode over BDD.

$$Fe^{2+} \rightarrow Fe^{3+} + e^- \tag{13}$$

$$S_2O_8^{2-} + 2Fe^{2+} \rightarrow 2SO_4^{2-} + 2Fe^{3+} \tag{14}$$

When analyzing the set of studied processes, it is clear that the most promising results of the Orange II decolorization are due to the use of the modified carbon cathode since the photodegration and anodic oxidation were only 12% and 27% color removal after 120 min of electrolysis, respectively. Thus, 77% of the Orange II decolorization with the modified carbon cathode and Pt anode was due to the cathode. The cathode-generated H_2O_2 [22] in the electro-Fenton and photoelectro-Fenton reactions transformed into hydroxyl radicals that attacked the organic molecule and destroyed the azo chromophore (—N═N—). Fig. 10 shows the absorption spectra of the decolorization of the Orange II solution by the Pt/photoelectro-Fenton process, in which the destruction of the azo chromophore and aromatic groups during the decolorization process can be observed [53].

Thus, future work will use the modified carbon cathode combined with the Pt anode for degradation because of its better performance in Orange II decolorization. Moreover, we found that the efficiency of Orange II decolorization obtained with the Pt/modified carbon pair was equal to or greater than other works reported in the literature [9,57–59].

4. Conclusions

$WO_{2.72}$/Vulcan XC72 and $WO_{2.72}$/Printex 6L have shown similar electrochemical activities toward hydrogen peroxide electrogeneration. The $WO_{2.72}$/Vulcan XC72 catalyst presented the highest relative ring current increase compared to the current recorded with unmodified carbon. After the addition of $WO_{2.72}$, the efficiency of H_2O_2 production increased from 67 to 87%, and the energy consumption decreased. This finding was attributed to a more acidic and hydrophilic surface of the modified Vulcan XC72 compared to Vulcan XC72. The wetability was clearly improved for both modified carbons as we can see in the results of contact angles. The positive effect of the nanoparticles was a synergic effect, since the entire surface of the modified carbons provides an enhancement of the amount of hydrogen peroxide produced. The electrocatalytic effect is in the entire material, a complete change of the

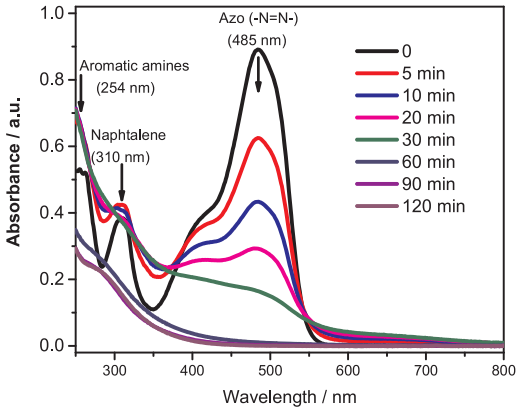

Fig. 10. UV–vis spectra of the solution of Orange II at different electrolysis times for the photoelectro-Fenton process.

chemical environment of the electrocatalyst for peroxide electrogenerated using modified carbons compared to unmodified ones

The best potential for H_2O_2 electrogeneration was −0.7 V vs Ag/AgCl for both $WO_{2.72}$/Vulcan XC72 GDE (1% w/w of W) and Vulcan XC72 GDE, which generated 479.1 mg L^{-1} and 160.5 mg L^{-1} H_2O_2 after 120 min of electrolysis, respectively. Moreover, the $WO_{2.72}$/Vulcan XC72 GDE showed lower power consumption (6.1 kW h kg^{-1} vs 13.8 kW h kg^{-1} of the unmodified Vulcan XC72 GDE) and higher current efficiency for electrogeneration of H_2O_2. All these results confirm the results of the ORR study. For the decolorization of the 0.260 mM Orange II solution, using $WO_{2.72}$/Vulcan XC72 GDE cathode, the efficiency has been found and is listed in increasing order as follows: PD < AO/Pt ≈ AO/BDD < EF/BDD < PEF/BDD < EF/Pt < PEF/Pt. The higher decolorization efficiency obtained with the Pt/modified carbon pair instead of the BDD/modified carbon pair was unexpected but is justified by the action of parasitic reactions on the BDD anode surface, which promote faster oxidation of Fe^{2+} to Fe^{3+} by the persulfate ion to obtain Fe^{3+} and sulfate, thus, decreasing the amount of Fe^{2+} to produce ·OH by Fenton's reaction. The results of the EF and PEF processes with Pt anode are promising since they presented efficiencies equal to or higher than similar studies of Orange II decolorization reported to date. Moreover, the results have shown that 77% of Orange II decolorization in the PEF and EF processes with a Pt anode occurs at the cathode. All these results show the high potential of the $WO_{2.72}$/Vulcan XC72 electrocatalyst.

Acknowledgments

The authors gratefully acknowledge the financial support received from Conselho Nacional de Desenvolvimento Científico e Tecnológico (CNPq) (grants 150532/2016-4, 406612/2013-7, 301492/2013-1, 465571/2014-0 INCT-DATREM), Coordenação de Aperfeiçoamento de Pessoal de Nível Superior (Capes) and Fundação de Amparo à Pesquisa do Estado de São Paulo (FAPESP) (grants 2015/10314-8, 2014/50945-4, 2016/01937-4, /2017/21846-6) and PROQUALIS – IFMA.

References

[1] S. Garcia-Segura, E. Brillas, Combustion of textile monoazo, diazo and triazo dyes by solar photoelectro-Fenton: decolorization, kinetics and degradation routes, Appl. Catal. B Environ. 181 (2016) 681–691.
[2] E. Brillas, C.A. Martínez-Huitle, Decontamination of wastewaters containing synthetic organic dyes by electrochemical methods. An updated review, Appl. Catal. B Environ. 166–167 (2015) 603–643.
[3] H. Zazou, N. Oturan, M. Sonmez-Celebi, M. Hamdani, M.A. Oturan, Mineralization of chlorobenzene in aqueous medium by anodic oxidation and electro-Fenton processes using Pt or BDD anode and carbon felt cathode, J. Electroanal. Chem. 774 (2016) 22–30.
[4] A. Moraes, M.H.M.T. Assumpção, R. Papai, I. Gaubeur, R.S. Rocha, R.M. Reis, et al., Use of a vanadium nanostructured material for hydrogen peroxide electrogeneration, J. Electroanal. Chem. 719 (2014) 127–132.
[5] F. Sopaj, M.A. Rodrigo, N. Oturan, F.I. Podvorica, J. Pinson, M.A. Oturan, Influence of the anode materials on the electrochemical oxidation efficiency. Application to oxidative degradation of the pharmaceutical amoxicillin, Chem. Eng. J. 262 (2015) 286–294.
[6] V.S. Antonin, L.S. Parreira, L.R. Aveiro, F.L. Silva, R.B. Valim, P. Hammer, et al., W@Au nanostructures modifying carbon as materials for hydrogen peroxide electrogeneration, Electrochim. Acta 231 (2017) 713–720.
[7] I. Sirés, E. Brillas, M.A. Oturan, M.A. Rodrigo, M. Panizza, Electrochemical advanced oxidation processes: today and tomorrow. A review, Environ. Sci. Pollut. Res. 21 (2014) 8336–8367.
[8] C. Salazar, C. Ridruejo, E. Brillas, J. Yánez, H.D. Mansilla, I. Sirés, Abatement of the fluorinated antidepressant fluoxetine (Prozac) and its reaction by-products by electrochemical advanced methods, Appl. Catal. B Environ. 203 (2017) 189–198.
[9] F. Yu, M. Zhou, X. Yu, Cost-effective electro-Fenton using modified graphite felt that dramatically enhanced on H2O2 electro-generation without external aeration, Electrochim. Acta 163 (2015) 182–189.
[10] A. Thiam, E. Brillas, J.A. Garrido, R.M. Rodríguez, I. Sirés, Routes for the electrochemical degradation of the artificial food azo-colour Ponceau 4R by advanced oxidation processes, Appl. Catal. B Environ. 180 (2016) 227–236.
[11] M.H.M.T. Assumpção, R.F.B. De Souza, R.M. Reis, R.S. Rocha, J.R. Steter, P. Hammer, et al., Low tungsten content of nanostructured material supported on carbon for the degradation of phenol, Appl. Catal. B Environ. 142–143 (2013) 479–486.
[12] F.C. Moreira, S. Garcia-Segura, R.A.R. Boaventura, E. Brillas, V.J.P. Vilar, Degradation of the antibiotic trimethoprim by electrochemical advanced oxidation processes using a carbon-PTFE air-diffusion cathode and a boron-doped diamond or platinum anode, Appl. Catal. B Environ. 160–161 (2014) 492–505.
[13] J.F. Carneiro, L.C. Trevelin, A.S. Lima, G.N. Meloni, M. Bertotti, P. Hammer, et al., Synthesis and characterization of ZrO2/C as electrocatalyst for oxygen reduction to H2O2, Electrocatalysis (2017) 189–195.
[14] W.R.P. Barros, R.M. Reis, R.S. Rocha, M.R.V. Lanza, Electrogeneration of hydrogen peroxide in acidic medium using gas diffusion electrodes modified with cobalt (II) phthalocyanine, Electrochim. Acta 104 (2013) 12–18.
[15] F.E. Fernades Rêgo, A.M. Sales Solano, I.C. Da Costa Soares, D.R. Da Silva, C.A. Martinez Huitle, M. Panizza, Application of electro-Fenton process as alternative for degradation of Novacron Blue dye, J. Environ. Chem. Eng. 2 (2014) 875–880.
[16] C.-Y. Chen, C. Tang, H.-F. Wang, C.-M. Chen, X. Zhang, X. Huang, et al., Oxygen reduction reaction on graphene in an electro-Fenton system: in situ generation of H_2O_2 for the oxidation of organic compounds, ChemSusChem 9 (2016) 1194–1199.
[17] H. Dong, H. Su, Z. Chen, H. Yu, H. Yu, Fabrication of electrochemically reduced graphene oxide modified gas diffusion electrode for in-situ electrochemical advanced oxidation process under mild conditions, Electrochim. Acta 222 (2016) 1501–1509.
[18] A. Khataee, A. Khataee, M. Fathinia, B. Vahid, S.W. Joo, Kinetic modeling of photoassisted-electrochemical process for degradation of an azo dye using boron-doped diamond anode and cathode with carbon nanotubes, J. Ind. Eng. Chem. 19 (2013) 1890–1894.
[19] G. Zhang, Q. Wei, X. Yang, A.C. Tavares, S. Sun, RRDE experiments on noble-metal and noble-metal-free catalysts: impact of loading on the activity and selectivity of oxygen reduction reaction in alkaline solution, Appl. Catal. B Environ. 206 (2017) 115–126.
[20] M. Dou, M. Hou, Z. Li, F. Wang, D. Liang, Z. Shao, et al., Pt/WO_3/C nanocomposite with parallel WO_3 nanorods as cathode catalyst for proton exchange membrane fuel cells, J. Energy Chem. 24 (2015) 39–44.
[21] M.H.M.T. Assumpção, R.F.B. De Souza, D.C. Rascio, J.C.M. Silva, M.L. Calegaro, I. Gaubeur, et al., A comparative study of the electrogeneration of hydrogen peroxide using Vulcan and Printex carbon supports, Carbon N. Y. 49 (2011) 2842–2851.
[22] F.C. Moreira, R.A.R. Boaventura, E. Brillas, V.J.P. Vilar, Electrochemical advanced oxidation processes: a review on their application to synthetic and real wastewaters, Appl. Catal. B Environ. 202 (2017) 217–261.
[23] M.H.M.T. Assumpção, A. Moraes, R.F.B. De Souza, I. Gaubeur, R.T.S. Oliveira, V.S. Antonin, et al., Low content cerium oxide nanoparticles on carbon for hydrogen peroxide electrosynthesis, Appl. Catal. A Gen. 411–412 (2012) 1–6.
[24] V.S. Antonin, M.H.M.T. Assumpção, J.C.M. Silva, L.S. Parreira, M.R.V. Lanza, M.C. Santos, Synthesis and characterization of nanostructured electrocatalysts based on nickel and tin for hydrogen peroxide electrogeneration, Electrochim. Acta 109 (2013) 245–251.
[25] C. Bruguera-Casamada, I. Sirés, E. Brillas, R.M. Araujo, Effect of electrogenerated hydroxyl radicals, active chlorine and organic matter on the electrochemical inactivation of Pseudomonas aeruginosa using BDD and dimensionally stable anodes, Sep. Purif. Technol. 178 (2017) 224–231.
[26] G. Coria, I. Sirés, E. Brillas, J.L. Nava, Influence of the anode material on the degradation of naproxen by Fenton-based electrochemical processes, Chem. Eng. J. 304 (2016) 817–825.
[27] H. Sarkka, A. Bhatnagar, M. Sillanpaa, Recent developments of electro-oxidation in water treatment - a review, J. Electroanal. Chem. 754 (2015) 46–56.
[28] C.A. Martínez-Huitle, M.A. Rodrigo, I. Sirés, O. Scialdone, Single and coupled electrochemical processes and reactors for the abatement of organic water pollutants: a critical review, Chem. Rev. 115 (2015) 13362–13407.
[29] A. Thiam, I. Sirés, J.A. Garrido, R.M. Rodríguez, E. Brillas, Effect of anions on electrochemical degradation of azo dye Carmoisine (Acid Red 14) using a BDD anode and air-diffusion cathode, Sep. Purif. Technol. 140 (2015) 43–52.
[30] B.C. Faust, R.G. Zepp, Photochemistry of Aqueous Iron(III)-polycarboxylate complexes: roles in the chemistry of atmospheric and surface waters, Environ. Sci. Technol. 27 (1993) 2517–2522.
[31] S. Shukla, S. Chaudhary, A. Umar, G.R. Chaudhary, S.K. Kansal, S.K. Mehta, Surfactant functionalized tungsten oxide nanoparticles with enhanced photocatalytic activity, Chem. Eng. J. 288 (2016) 423–431.
[32] U.A. Paulus, T.J. Schmidt, H.A. Gasteiger, R.J. Behm, Oxygen reduction on a high-surface area Pt/Vulcan carbon catalyst: a thin-film rotating ring-disk electrode study, J. Electroanal. Chem. 495 (2001) 134–145.
[33] J.F. Carneiro, R.S. Rocha, P. Hammer, R. Bertazzoli, M.R.V. Lanza, Hydrogen peroxide electrogeneration in gas diffusion electrode nanostructured with Ta2O5, Appl. Catal. A Gen. 517 (2016) 161–167.
[34] J.C. Forti, R.S. Rocha, M.R.V. Lanza, R. Bertazzoli, Electrochemical synthesis of hydrogen peroxide on oxygen-fed graphite/PTFE electrodes modified by 2-ethylanthraquinone, J. Electroanal. Chem. 601 (2007) 63–67.
[35] Z. Qiang, J. Chang, C. Huang, Electrochemical generation of hydrogen peroxide from dissolved oxygen in acidic solutions, Water Res. 36 (2002) 85–94.
[36] G. Hai, J. Huang, L. Cao, Y. Jie, J. Li, X. Wang, et al., Influence of oxygen deficiency on the synthesis of tungsten oxide and the photocatalytic activity for the removal of organic dye, J. Alloys Compd. 690 (2017) 239–248.
[37] M. Sriyudthsak, S. Supothina, Humidity-insensitive and low oxygen dependence tungsten oxide gas sensors, Sens. Actuators B Chem. 113 (2006) 265–271.
[38] A.V. Naumkin, A. Kraut-Vass, S.W. Gaarenstroom, C.J. Powell, NIST X-ray Photoelectron Spectroscopy Database, (2012).
[39] A. Zdziennicka, K. Szymczyk, J. Krawczyk, B. Janczuk, Some remarks on the solid

surface tension determination from contact angle measurements, Appl. Surf. Sci. 405 (2017) 88–101.
[40] S. Banerjee, D.D. Dionysiou, S.C. Pillai, Self-cleaning applications of TiO2 by photo-induced hydrophilicity and photocatalysis, Appl. Catal. B: Environ. 177 (2015) 396–428.
[41] A.S. Martins, P.J.M. Cordeiro-Junior, L. Nuñez, M.R. de Vasconcelos Lanza, A simple method for the electrodeposition of WO_3 in TiO_2 nanotubes: influence of the amount of tungsten on photoelectrocatalytic activity, Electrocatalysis 8 (2017) 115–121.
[42] B.E. Conway, J.O. Bockris, E. Yeager, S.U.M. Khan, R.E. White, Comprehensive Treatise of Electrochemistry: Kinetics and Mechanisms of Electrode Processes, New York (1983).
[43] A. Alvarez-Gallegos, D. Pletcher, The removal of low level organics via hydrogen peroxide formed in a reticulated vitreous carbon cathode cell, part 1. The electro-synthesis of hydrogen peroxide in aqueous acidic solutions, Electrochim. Acta 44 (1998) 853–861.
[44] L. Demarconnay, C. Coutanceau, J.M. Léger, Electroreduction of dioxygen (ORR) in alkaline medium on Ag/C and Pt/C nanostructured catalysts - effect of the presence of methanol, Electrochim. Acta 49 (2004) 4513–4521.
[45] H. Meng, P.K. Shen, Novel Pt-free catalyst for oxygen electroreduction, Electrochem. Commun. 8 (2006) 588–594.
[46] Y. Feng, T. He, N. Alonso-vante, Oxygen reduction reaction on carbon-supported $CoSe_2$ nanoparticles in an acidic medium, Electrochim. Acta 54 (2009) 5252–5256.
[47] Y. Wang, Y. Liu, K. Wang, S. Song, P. Tsiakaras, H. Liu, Preparation and characterization of a novel KOH activated graphite felt cathode for the electro-Fenton process, Appl. Catal. B Environ. 165 (2015) 360–368.
[48] G. Xia, Y. Lu, H. Xu, Electrogeneration of hydrogen peroxide for electro-Fenton via oxygen reduction using polyacrylonitrile-based carbon fiber brush cathode, Electrochim. Acta 158 (2015) 390–396.
[49] H. Xue, Y. Xing, Y. Yin, T. Zhang, B. Zhang, Y. Zhang, et al., Application of an enzyme immunoassay for the quantitative determination of azo dye (Orange II) in food products, Food Addit. Contam. Part A 29 (2012) 1840–1848.
[50] S.A. Ong, E. Toorisaka, M. Hirata, T. Hano, Decolorization of azo dye (Orange II) in a sequential UASB-SBR system, Sep. Purif. Technol. 42 (2005) 297–302.
[51] J. Herney-Ramirez, M. Lampinen, M.A. Vicente, C.A. Costa, L.M. Madeira, Experimental design to optimize the oxidation of orange II dye solution using a clay-based fenton-like catalyst, Ind. Eng. Chem. Res. 47 (2008) 284–294.
[52] M.L. Rache, A.R. García, H.R. Zea, A.M.T. Silva, L.M. Madeira, J.H. Ramírez, Azo-dye orange II degradation by the heterogeneous Fenton-like process using a zeolite Y-Fe catalyst—Kinetics with a model based on the Fermi's equation, Appl. Catal. B Environ. 146 (2014) 192–200.
[53] P. Liang, M. Rivallin, S. Cerneaux, S. Lacour, E. Petit, M. Cretin, Coupling cathodic electro-Fenton reaction to membrane filtration for AO7 dye degradation: a successful feasibility study, J. Membr. Sci. 510 (2016) 182–190.
[54] C. Trellu, Y. Péchaud, N. Oturan, E. Mousset, D. Huguenot, E.D. van Hullebusch, et al., Comparative study on the removal of humic acids from drinking water by anodic oxidation and electro-Fenton processes: mineralization efficiency and modelling, Appl. Catal. B Environ. 194 (2016) 32–41.
[55] V.S. Antonin, S. Garcia-Segura, M.C. Santos, E. Brillas, Degradation of Evans Blue diazo dye by electrochemical processes based on Fenton's reaction chemistry, J. Electroanal. Chem. 747 (2015) 1–11.
[56] I. Sirés, J.A. Garrido, R.M. Rodríguez, E. Brillas, N. Oturan, M.A. Oturan, Catalytic behavior of the Fe^{3+}/Fe^{2+} system in the electro-Fenton degradation of the antimicrobial chlorophene, Appl. Catal. B Environ. 72 (2007) 382–394.
[57] J. Zheng, Z. Gao, H. He, S. Yang, C. Sun, Efficient degradation of acid Orange 7 in aqueous solution by iron ore tailing Fenton-like process, Chemosphere 150 (2016) 40–48.
[58] C. Zhang, L. Liu, W. Li, J. Wu, F. Rong, D. Fu, Electrochemical degradation of acid Orange II dye with boron-doped diamond electrode: role of operating parameters in the absence and in the presence of NaCl, J. Electroanal. Chem. 726 (2014) 77–83.
[59] F. Luo, D. Yang, Z. Chen, M. Megharaj, R. Naidu, One-step green synthesis of bimetallic Fe/Pd nanoparticles used to degrade Orange II, J. Hazard. Mater. 303 (2016) 145–153.